J|A|C|S ARTICLES

Published on Web 12/16/2009

Δ^{12}-Prostaglandin J_2 as a Product and Ligand of Human Serum Albumin: Formation of an Unusual Covalent Adduct at His146

Satoru Yamaguchi,[†] Giancarlo Aldini,[‡] Sohei Ito,[§] Nozomi Morishita,[†] Takahiro Shibata,[†] Giulio Vistoli,[‡] Marina Carini,[‡] and Koji Uchida*,[†]

Graduate School of Bioagricultural Sciences, Nagoya University, Nagoya 464-8601, Japan, Dipartimento di Scienze Farmaceutiche "Pietro Pratesi", University of Milan, I-20131, Milan, Italy, and School of Food and Nutritional Sciences, University of Shizuoka, Shizuoka 422-8526, Japan

Received October 17, 2009; E-mail: uchidak@agr.nagoya-u.ac.jp

Abstract: Human serum albumin (HSA), the most abundant protein in plasma, has a very unique function, catalyzing the conversion of prostaglandin J_2 (PGJ_2), a dehydration product of PGD_2, to yield Δ^{12}-PGJ_2. These PGD_2 metabolites are actively transported into cells and accumulated in the nuclei, where they act as potent inducers of cell growth inhibition and cell differentiation, and exhibit their own unique spectrum of biological effects. The facts that (i) arachidonic acid metabolites bind to human serum albumin (HSA) and the metabolism of these molecules is altered as a result of binding, (ii) HSA catalyzes the transformation of PGJ_2 into Δ^{12}-PGJ_2, and (iii) Δ^{12}-PGJ_2 is stable in serum suggest that HSA may bind and stabilize Δ^{12}-PGJ_2 in a specific manner. A molecular interaction analysis using surface plasmon resonance (Biacore) indeed suggested the presence of a specific Δ^{12}-PGJ_2-binding site in HSA. To investigate the molecular details of the binding of this PGD_2 metabolite to albumin, we analyzed the cocrystal structure of the HSA$-\Delta^{12}$-PGJ_2-myristate complex by X-ray crystallography and found that two Δ^{12}-PGJ_2 molecules bind to a primary site in subdomain IB of the protein. The electron density results suggested that one of the two Δ^{12}-PGJ_2 molecules that specifically bind to the site covalently interacted with a histidine residue (His146). Using nano-LC-MS/MS analysis of the HSA$-\Delta^{12}$-PGJ_2 complex, the formation of an unusual Δ^{12}-PGJ_2-histidine adduct at His146 was confirmed. Thus, our crystallographic and mass spectrometric analyses of the HSA$-\Delta^{12}$-PGJ_2 complex provided intriguing new insights into the molecular details of how this electrophilic ligand interacts with its primary producer and transporter.

Introduction

The prostaglandins (PGs) are a family of structurally related molecules that are produced by cells in response to a variety of extrinsic stimuli and regulate cellular growth, differentiation, and homeostasis.[1,2] Among them, PGD_2 is a major cyclooxygenase product in a variety of tissues and cells and has marked effects on a number of biological processes, including platelet aggregation, relaxation of vascular and nonvascular smooth muscles, and nerve cell functions.[3] PGD synthase catalyzes the isomerization of the 9,10-endoperoxide group of PGH_2, a precursor of prostanoids, to produce PGD_2. Two distinct types of PGD synthases have been identified: the lipocalin enzyme (L-PGDS) and hematopoietic enzyme (H-PGDS). Although L-PGDS is expressed in the central nervous system and male genital organs of various mammals, H-PGDS is widely expressed in peripheral tissues, as well as in antigen-presenting cells, mast cells, and megakaryocytes.[4] The PGs are physiologically present in body fluids in picomolar-to-nanomolar concentrations;[5] however, the arachidonate metabolism is significantly increased under several pathological conditions including hyperthermia, infection, and inflammation,[6] and local PG concentrations in the micromolar range have been detected at sites of acute inflammation.[7] The two major enzymatic pathways responsible for the catabolism of PGD_2 are an 11-ketoreductase and NADP-linked 15-hydroxy-PG-dehydrogenase.[3,8] The former pathway leads to the production of 11β-PGF_{2a}. The second pathway leads to the formation of 13,14-dihydro-15-keto-PGD_2, which does not appear to be biologically active.

PGD_2 is known to be relatively unstable and readily undergoes dehydration in vivo and in vitro to yield biologically active PGs

[†] Nagoya University.
[‡] University of Milan.
[§] University of Shizuoka.

(1) Smith, W. L. *Biochem. J.* **1989**, *259*, 315–324.
(2) Smith, W. L. *Am. J. Physiol.* **1992**, *263*, F181–191.
(3) Giles, H.; Leff, P. *Prostaglandins* **1988**, *35*, 277–300.
(4) Urade, Y.; Eguchi, N. *Prostaglandins Other Lipid Mediators* **2002**, *68−69*, 375–382.
(5) Fukushima, M. *Eicosanoids* **1990**, *3*, 189–199.
(6) Herschman, H. R.; Reddy, S. T.; Xie, W. *Adv. Exp. Med. Biol.* **1997**, *407*, 61–66.
(7) Offenbacher, S.; Odle, B. M.; Van Dyke, T. E. *J. Periodontal Res.* **1986**, *21*, 101–112.
(8) Urade, Y.; Watanabe, K.; Eguchi, N.; Fujii, Y.; Hayaishi, O. *J. Biol. Chem.* **1990**, *265*, 12029–12035.

10.1021/ja908878n

of the J_2 series, such as PGJ_2, Δ^{12}-PGJ_2, and 15d-PGJ_2.[9,10] These cyclopentenone-type PGs (cyPGs) are actively transported into cells and accumulated in the nuclei, where they act as potent inducers of cell growth inhibition and cell differentiation, and exhibit their own unique spectrum of biological effects, including the inhibition of cell cycle progression, the suppression of viral replication, the induction of the heat shock protein expression, and the stimulation of osteogenesis.[11] In addition, the physiopathological relevance of the enhanced synthesis of cyPGs in activated macrophages has been speculated to represent a mechanism in which they function as a feedback regulator of the inflammatory responses.[12−14]

The general instability of the PGs in aqueous media has made it difficult to unravel the many biological roles played by these highly active signaling molecules. It became apparent early on in prostaglandin research that proteins in the blood might play an important role in modulating the biological activities of these compounds by binding to and stabilizing or destabilizing certain PGs. A series of binding studies using radiolabeled PGE_1, PGE_2, PGA_2, and PGF_2 found that the only plasma protein that significantly binds to the above prostaglandins is human serum albumin (HSA).[15] HSA is the most abundant protein in plasma, where it acts as a transporter of an exceptionally broad spectrum of compounds that are predominantly fatty acids, but also amino acids, bile acids, and steroids.[16] It is also capable of binding and transporting a wide range of therapeutic substances. Its binding abilities have been probed in a number of studies, and crystal structures are available for HSA in complexes with fatty acids,[17,18] hemin,[19] and local anesthetics.[20] Although the affinity of HSA for a variety of biologically active arachidonic acid metabolites is relatively low,[21,22] the high serum HSA concentration makes these interactions physiologically significant. HSA has been shown to stabilize PGI_2,[23] an unstable but potent inhibitor of platelet aggregation derived from PGH_2. However, HSA stabilizes the potent stimulant of irreversible platelet aggregation TXA_2,[24] enhancing its activity. In addition, HSA binds LTA_4,[25] the unstable precursor of most leukotrienes, preventing its rapid nonenzymatic degradation to biologically inactive metabolites in aqueous media.

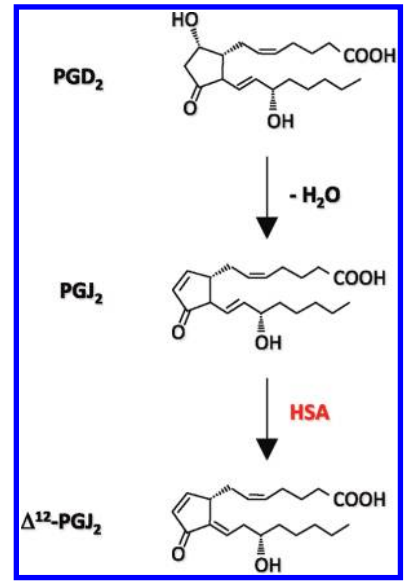

Figure 1. HSA-dependent PGD_2 metabolic pathway.

On the other hand, HSA is known to be an endogenous catalyst of the PGD_2 metabolism. HSA catalyzes the conversion of PGH_2 to PGD_2.[26] In addition, in aqueous solutions containing HSA, PGJ_2 isomerizes to yield Δ^{12}-PGJ_2 (Figure 1).[27] Hirata et al. have previously shown that the injection of monkeys with a single dose of PGD_2 indeed results in a dramatic increase in the output of urinary Δ^{12}-PGJ_2, whereas treatment with a cyclooxygenase inhibitor results in a significant decrease in urinary levels of Δ^{12}-PGJ_2.[28] They have also shown that Δ^{12}-PGJ_2 is present in significant quantities in human urine. These data provided evidence that Δ^{12}-PGJ_2 is a natural PGD_2 metabolite that is formed in vivo and excreted in the urine. In a later study, Δ^{12}-PGJ_2 has been identified as substance produced by murine bone marrow-derived mast cells.[29] These findings and the fact that Δ^{12}-PGJ_2 is stable in serum suggest that Δ^{12}-PGJ_2 may be produced and actively carried by HSA in the bloodstream and transported into cells to exhibit its biological effects. In this Article, we describe the three-dimensional structure of HSA complexed with Δ^{12}-PGJ_2 and show that, despite the repeating domain structure of the protein, two molecules of Δ^{12}-PGJ_2 uniquely bind at a fatty acid binding site. We also show that one of the two Δ^{12}-PGJ_2 molecules covalently interacts with a histidine residue to form an unusual Δ^{12}-PGJ_2-histidine adduct. These data suggest an explanation for observations that Δ^{12}-PGJ_2 and related PGs show a unique spectrum of biological effects.

Results

Molecular Interaction between HSA and Δ^{12}-PGJ_2. We first checked the PGJ_2-isomerization activity of the commercially obtained HSA (fatty acid and globulin free, purity 99%) used

(9) Fitzpatrick, F. A.; Wynalda, M. A. *J. Biol. Chem.* **1983**, *258*, 11713–11718.
(10) Kikawa, Y.; Narumiya, S.; Fukushima, M.; Wakatsuka, H.; Hayaishi, O. *Proc. Natl. Acad. Sci. U.S.A.* **1984**, *81*, 1317–1321.
(11) Fukushima, M. *Prostaglandins, Leukotrienes Essent. Fatty Acids* **1992**, *47*, 1–12.
(12) Gilroy, D. W.; Colville-Nash, P. R.; Willis, D.; Chivers, J.; Paul-Clark, M. J.; Willoughby, D. A. *Nat. Med.* **1999**, *5*, 698–701.
(13) Cuzzocrea, S.; Wayman, N. S.; Mazzon, E.; Dugo, L.; Di Paola, R.; Serraino, I.; Britti, D.; Chatterjee, P. K.; Caputi, A. P.; Thiemermann, C. *Mol. Pharmacol.* **2002**, *61*, 997–1007.
(14) Itoh, K.; Mochizuki, M.; Ishii, Y.; Ishii, T.; Shibata, T.; Kawamoto, Y.; Kelly, V.; Sekizawa, K.; Uchida, K.; Yamamoto, M. *Mol. Cell. Biol.* **1972**, *24*, 36–45.
(15) Raz, A. *Biochem. J.* **1972**, *130*, 631–636.
(16) Peters T. *All About Albumin: Biochemistry, Genetics and Medical Applications*; Academic Press: San Diego, CA, 1995.
(17) Curry, S.; Mandelkow, H.; Brick, P.; Franks, N. *Nat. Struct. Biol.* **1998**, *5*, 827–835.
(18) Bhattacharya, A. A.; Grüne, T.; Curry, S. *J. Mol. Biol.* **2000**, *303*, 721–732.
(19) Wardell, M.; Wang, Z.; Ho, J. X.; Robert, J.; Ruker, F.; Ruble, J.; Carter, D. C. *Biochem. Biophys. Res. Commun.* **2002**, *291*, 813–819.
(20) Zunszain, P. A.; Ghuman, J.; Komatsu, T.; Tsuchida, E.; Curry, S. *BMC Struct. Biol.* **2003**, *3*, 6.
(21) Unger, W. G. B. *J. Pharm. Pharm. Sci.* **1972**, *24*, 470–477.
(22) Gueriguian, J. L. *J. Pharmacol. Exp. Ther.* **1976**, *197*, 391–401.
(23) Wynalda, N. A.; Fitzpatrick, F. A. *Prostaglandins Other Lipid Mediators* **1980**, *20*, 853–861.
(24) Folco, G.; Granstrom, E.; Kindahl, H. *FEBS Lett.* **1977**, *82*, 321–324.
(25) Fitzpatrick, F. A.; Morton, D. R.; Wynalda, M. A. *J. Biol. Chem.* **1981**, *257*, 4680–4683.
(26) Watanabe, T.; Narumiya, S.; Shimizu, T.; Hayaishi, O. *J. Biol. Chem.* **1982**, *257*, 14847–14853.
(27) Shibata, T.; Kondo, M.; Osawa, T.; Shibata, N.; Kobayashi, M.; Uchida, K. *J. Biol. Chem.* **2002**, *277*, 10459–10466.
(28) Hirata, Y.; Hayashi, H.; Ito, S.; Kikawa, Y.; Ishibashi, M.; Sudo, M.; Miyazaki, H.; Fukushima, M.; Narumiya, S.; Hayaishi, O. *J. Biol. Chem.* **1988**, *263*, 16619–16625.
(29) Haberl, C.; Hultner, L.; Flugel, A.; Falk, M.; Geuenich, S.; Wilmanns, W.; Denzlinger, C. *Mediators Inflammation* **1988**, *7*, 79–84.

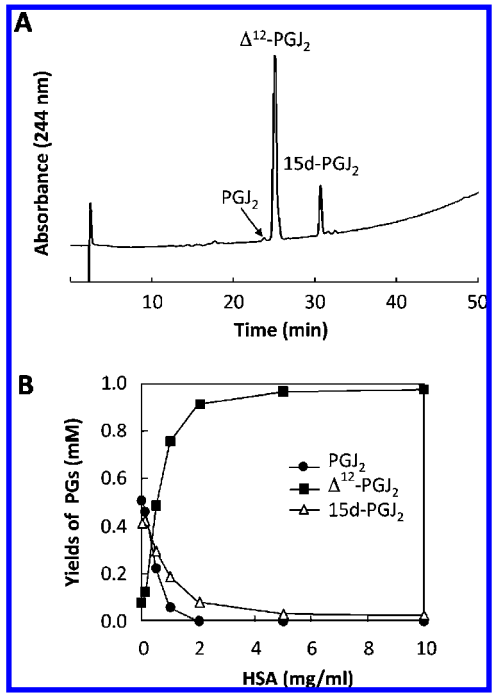

Figure 2. Conversion of PGJ_2 by Δ^{12}-PGJ_2. (A) HPLC profile of PGJ_2 metabolites. PGJ_2 (1 mM) was incubated in PBS containing HSA (10 mg/mL) for 24 h. PGJ_2 and its metabolites were separated on a ChiralPak AD-RH column (0.46 × 15 cm) eluted with a linear gradient of acetonitrile/water/acetic acid (90/10/0.01, by vol.) (solvent A) − acetonitrile (solvent B) (time = 0−5 min, 100% A; 60 min, 0% A), at a flow rate of 0.8 mL/min. The elution profiles were monitored by UV absorbance at 244 nm. (B) Dose-dependent conversion of PGJ_2 to Δ^{12}-PGJ_2 by HSA. PGJ_2 was incubated in PBS containing HSA (0−10 mg/mL) for 24 h. Symbols: △, PGJ_2; ■, Δ^{12}-PGJ_2; ●, 15d-PGJ_2.

in this study. PGJ_2 was incubated in PBS containing HSA, and the products were analyzed by chiral-phase HPLC. It was observed that PGJ_2 was converted to both 15d-PGJ_2 and Δ^{12}-PGJ_2 in the presence of HSA (Figure 2A). The isomerization of PGJ_2 to Δ^{12}-PGJ_2 was dependent on the incubation time and the concentration of HSA; when HSA was present in excess, PGJ_2 was almost stoichiometrically converted to Δ^{12}-PGJ_2 (Figure 2B).

Despite the fact that HSA is a fatty acid-binding protein, the protein is not known to bind Δ^{12}-PGJ_2. Therefore, we studied the HSA−Δ^{12}-PGJ_2 interaction using surface plasmon resonance analysis. Δ^{12}-PGJ_2 was subjected to an exchange reaction to preload it and tested for an interaction with HSA immobilized on a Biacore chip. Δ^{12}-PGJ_2 showed rapid binding and dissociation kinetics with a dissociation constant of 420 μM (Figure 3). Of interest, at higher concentrations over 125 μM, a fraction of Δ^{12}-PGJ_2 remained bound to the anchored HSA upon prolonged exposure, suggesting that Δ^{12}-PGJ_2 might covalently interact with HSA. Moreover, HSA recognizes Δ^{12}-PGJ_2 with an R_{max} (the total number of accessible binding sites) of 19.1 resonance units, which was almost comparable to the theoretical R_{max} of 18.7 resonance units when the protein binds one Δ^{12}-PGJ_2 molecule. These findings suggest that HSA may have a specific binding site for Δ^{12}-PGJ_2.

Crystallographic Analysis and Δ^{12}-PGJ_2 Binding Sites. To investigate the molecular details of the binding of the PGD_2 metabolite to the protein, we prepared the Δ^{12}-PGJ_2 complex of HSA and analyzed it by X-ray crystallography. The Δ^{12}-PGJ_2−HSA complexes were prepared by incubating the protein with a 5 molar excess of Δ^{12}-PGJ_2 with or without myristate.

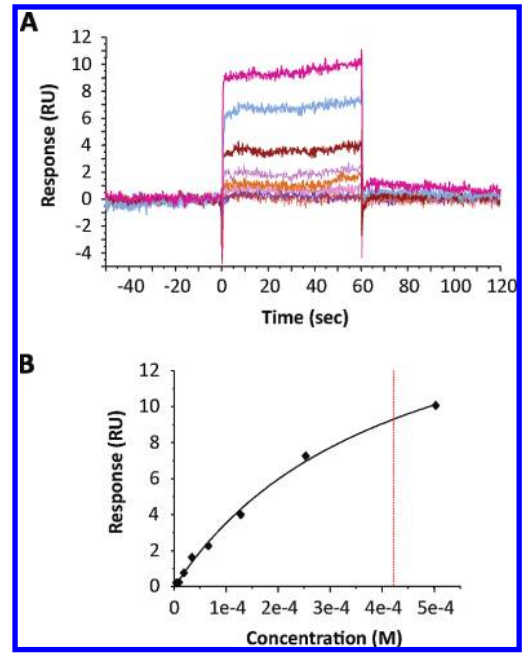

Figure 3. Surface plasmon resonance (Biacore) detection of the interaction between HSA and Δ^{12}-PGJ_2. (A) Responses from injections at 3.9, 7.8, 15.6, 31.3, 62.5, 125, 250, and 500 μM. Sensorgram are double-referenced and solvent-corrected. (B) Equilibrium binding responses plotted versus Δ^{12}-PGJ_2 concentration and fitted to a simple binding isotherm to yield an affinity of 420 μM.

The Δ^{12}-PGJ_2−HSA crystal, diffracted up to a 2.5 Å resolution, showed a positive electron density that protruded from the side-chain of His146. However, the Δ^{12}-PGJ_2 binding configurations were unclear because of the poor electron densities for the suspected Δ^{12}-PGJ_2 molecules. An improved procedure involving the addition of Δ^{12}-PGJ_2 to the harvesting solution and cocrystallization with myristate revealed that two Δ^{12}-PGJ_2 molecules (Δ^{12}-PGJ_2-1 and Δ^{12}-PGJ_2-2) exist in the subdomain IB (Figure 4).

The omit maps and $2F_o - F_c$ maps at a 2.2 Å resolution also showed clear densities for the two Δ^{12}-PGJ_2 molecules (Figure 5A and Supporting Information Figure S1). A break in the electron density around the cyclopentenone ring of Δ^{12}-PGJ_2-1, especially in chain A, suggested a competition against the myristate. However, the shape of the density, which had a significant broadening at one end, clearly indicated the position of the carboxyl moiety and thus defined the orientation of the bound Δ^{12}-PGJ_2 molecules. Figure 5B shows that the cyclopentenone ring and both tails of Δ^{12}-PGJ_2-1 are rigidly anchored by HSA. The Δ^{12}-PGJ_2-1 binding site has a large interaction surface area up to 447 Å^2, allowing shape-adaptability with Δ^{12}-PGJ_2 through a specific hydrophobic interaction. It also appears that Δ^{12}-PGJ_2-1 binds at this site in the same orientation with other saturated medium- and long-chain fatty acids.[18] The calculated interaction surface area of Δ^{12}-PGJ_2-2 with HSA was significantly low (258 Å^2), and its carboxyl group and methylene tail were disordered, especially in chain B. The bond distance between the imidazole nitrogen N^{τ} and cyclopentenone ring (2.25 Å in chain A) and positive electron densities near the His146 in chain B (Figure 5A and Supporting Information Figure S1, panel D) strongly suggest that His146 in both monomers may covalently bind to Δ^{12}-PGJ_2-2. No other significant interaction was observed between Δ^{12}-PGJ_2-2 and HSA, suggesting that the covalent bond may be indispensable to sustaining the PG molecule (Figure 5A). In addition, no

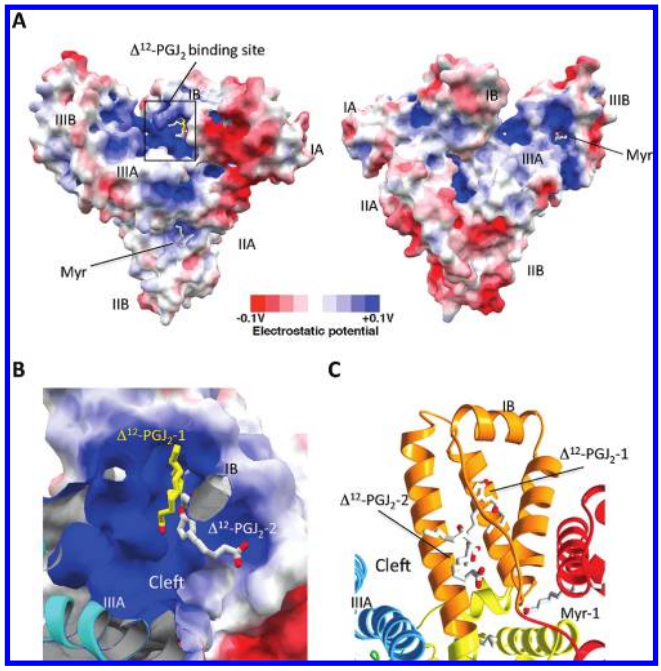

Figure 4. Crystal structure of HSA complexed with Δ^{12}-PGJ_2 and myristate. (A) Electrostatic potential at the molecular surface of both sides of the complex and location of myristate and Δ^{12}-PGJ_2 binding sites. HSA is composed of three homologous domains (I−III), each of which is divided into A and B subdomains. Two Δ^{12}-PGJ_2 and two of the six molecules of myristic acid found to bind to HSA are visible in these figures. The electrostatic potential is represented on a color scale from blue for a positive potential, white for neutral, to red for a negative potential. Bound Δ^{12}-PGJ_2 and myristic acid (Myr) are shown in a stick representation with atoms colored by atom-type: carbon, yellow for Δ^{12}-PGJ_2-1 and white for Δ^{12}-PGJ_2-2; oxygen, red. (B) Close-up view of Δ^{12}-PGJ_2 binding site. Two Δ^{12}-PGJ_2 molecules bound to HSA are shown as a stick model. Cross-sections of the protein are shown in a gray color, and the α-helix of the subdomain IIIA at the cross-section is colored cyan. The Δ^{12}-PGJ_2 binding site is located at the positively charged and hydrophobic groove face of the subdomain IIIA. Near the Δ^{12}-PGJ_2 binding site, negatively charged interdomain cleft was reported to bind to some drugs. (C) Schematic representation of Δ^{12}-PGJ_2 binding site. The subdomains are color-coded as follows: IA, red; IB, orange; IIA, yellow; IIIA, cyan.

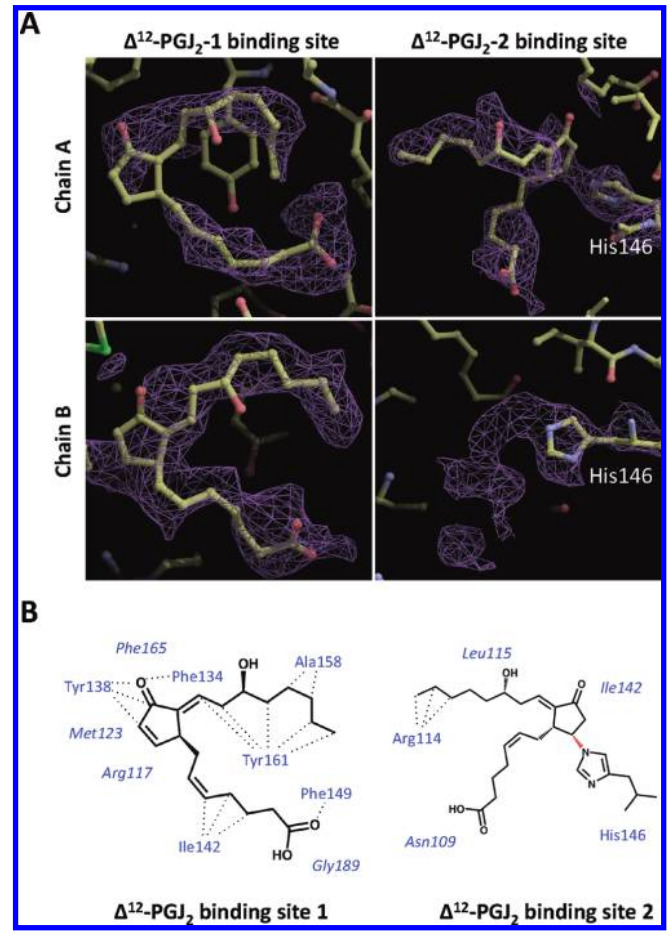

Figure 5. The omit maps and $2 > F_o - F_c$ electron density maps for Δ^{12}-PGJ_2 binding in subdomain IB of the HSA−Δ^{12}-PGJ_2-myristate complex. (A) Close-up views of the omit maps (contoured at 0.9 σ), showing two Δ^{12}-PGJ_2 molecules bound to the subdomains IB of both monomers (chains A and B). The bound Δ^{12}-PGJ_2 and HSA are shown in a stick representation with atoms colored by atom-type: carbon, yellow; oxygen, red; nitrogen, blue. In the discussion of the fatty acid binding sites, we have adopted the site-numbering scheme that was established by Curry et al.[17,59] The Δ^{12}-PGJ_2-1 binding site is precisely located at the fatty acid binding site 1, and Δ^{12}-PGJ_2-1 binds at this site in the same orientation with polyunsaturated fatty acids.[59] (B) Representations of the interaction between Δ^{12}-PGJ_2 and HSA. Left, a representation of the interaction between Δ^{12}-PGJ_2-1 and HSA. Right, a representation of the interaction between Δ^{12}-PGJ_2-2 and HSA. The residues located near the bound Δ^{12}-PGJ_2 are also illustrated in italics. The covalent bond between Δ^{12}-PGJ_2-2 and His146 is denoted by a red line. The chiral conformation around the carbon atom covalently bound to His146 is (*R*).

electron density for Δ^{12}-PGJ_2 was observed in the other fatty acid binding sites or coexisted with the myristate molecule (Supporting Information Figure S2), suggesting that Δ^{12}-PGJ_2 can primary replace myristate and bind at the subdomain IB. The line shape of these sites or the size of the grooves except for fatty acid binding sites 1 and 6 may prevent the binding of the D-shaped Δ^{12}-PGJ_2 molecule.

On the other hand, HSA has a highly reactive free sulfhydryl group at position 34 (Cys34), which is a major ligand-binding site for thiol-containing compounds and α,β-unsaturated molecules.[30] However, no modification of the cysteine residue was observed in the crystal structure of the HSA−Δ^{12}-PGJ_2 and HSA−Δ^{12}-PGJ_2-myristate complexes (Supporting Information Figure S3).

MALDI-TOF MS and Direct Infusion ESI-MS Analyses of the HSA−Δ^{12}-PGJ_2 Complex. The crystallographic analyses of the HSA−Δ^{12}-PGJ_2 complex suggested the presence of Δ^{12}-PGJ_2-His146 adduct in HSA. To confirm this result, the native and Δ^{12}-PGJ_2-treated HSA were analyzed by MALDI-TOF MS. The analysis of the native HSA revealed a peak with *m/z* 67 473, whereas the protein incubated with 1 mM Δ^{12}-PGJ_2 had a peak with *m/z* 67 988 (Figure 6A). The peak differs in molecular mass by approximately 500 Da, which is close to the molecular mass of Δ^{12}-PGJ_2 (334 Da), suggesting the addition of at least one molecule of the Δ^{12}-PGJ_2 per protein. To confirm the formation of the Δ^{12}-PGJ_2-HSA covalent adduct, the native and the Δ^{12}-PGJ_2-treated HSA were analyzed by direct infusion ESI-MS analysis. Figure 6B represents the positive-ion ESI mass spectrum of serum HSA (scan range *m/z* 600−2000), showing multiple charged peaks ranging from *m/z* 1055.92 to *m/z* 1955.17 and corresponding to the addition of 63 to 34 protons. To further enhance the MS resolution, a reduced scan range *m/z* 1410−1500 was used to acquire the MS spectrum for 10 min at an *m/z* 0.5 resolution. Figure 6C shows the ESI-MS spectrum in the positive-ion mode of the native HSA, characterized by three abundant ions at *m/z* 1414.7, 1445.4, and 1477.5, and attributed

(30) Aldini, G.; Gamberoni, L.; Orioli, M.; Beretta, G.; Regazzoni, L.; Maffei Facino, R.; Carini, M. *J. Mass Spectrom.* **2006**, *41*, 1149–1161.

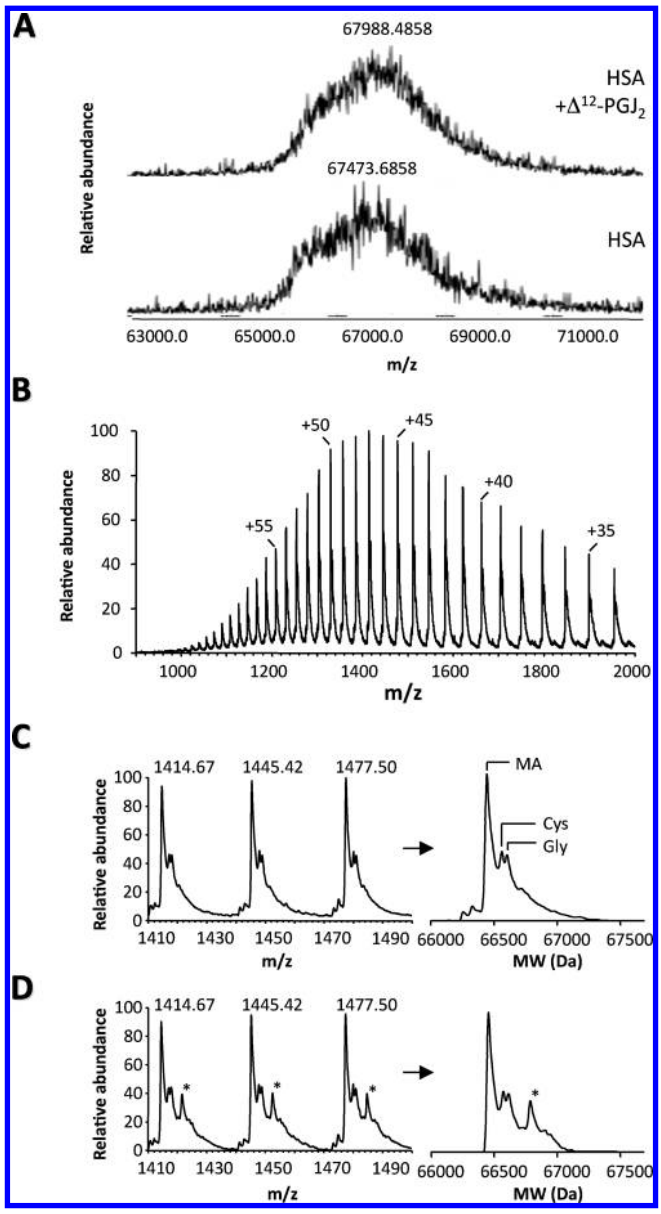

Figure 6. Covalent binding of Δ^{12}-PGJ_2 to HSA. (A) MALDI-TOF-MS analysis of HSA treated with and without Δ^{12}-PGJ_2. (B-D) ESI-MS spectrum (linear ion-trap as mass analyzer) of isolated serum HSA using mass ranges *m/z* 900−2000 (panel B) and *m/z* 1410−1500 (panels C and D). On the right side are depicted the deconvoluted spectra. HSA was incubated for 3 h at 37 °C in the absence (panel C) and presence of Δ^{12}-PGJ_2 (panel D) at the molar ratio of HSA:Δ^{12}-PGJ_2 = 1:1. In panel C, MA indicates mercapto albumin, and Cys and Gly represent the cysteinylated (66 566 Da) and glycated (66 610 Da) forms of HSA, respectively. In panel D, "*" indicates the signals relative to the monoadduct.

to the +47, +46, and +45 multicharged ions of the native HSA (mercapto-albumin; compound MA). As previously reported working with a triple-stage quadrupole system,[30] the MS spectrum is also characterized by two other ions series relative to the cysteinylated (compound Cys; +120 Da found; +119 Da theoretical) and glycated forms (compound Gly, +164 Da found; +162 theoretical), reaching a relative abundance of 30−35% with respect to the native HSA. The deconvoluted spectra (right panels) show molecular weights of 66 446, 66 566, and 66 610 Da for compounds MA, Cys, and Gly, respectively. When HSA was incubated in the presence of Δ^{12}-PGJ_2 at a molar ratio 1:1 for 180 min at 37 °C, an additional ion series (marked by "*") was quite detectable (relative abundance ≈ 40% with respect to mercapto-albumin) (Figure 6D). A deconvolution analysis indicated a MW 66 778 [+332 Da in respect to native HSA (66 446 Da)], which can be attributed to the Δ^{12}-PGJ_2-Michael adduct (theoretical mass increment +334.5 Da).

Identification of the Δ^{12}-PGJ_2-Binding Site Using Nano-LC-MS/MS. The Δ^{12}-PGJ_2-mediated structural modification(s) of HSA were further characterized by a nano-LC-MS/MS analysis of the incubated samples after reduction with $NaBH_4$, an established procedure for adduct stabilization, followed by enzymatic digestion. When trypsin was used as the proteolytic enzyme, peptide mass mapping provided identification of the peptides, accounting for approximately 80% of the protein sequence as previously reported.[30] The Δ^{12}-PGJ_2-adducted peptide was first identified by using a semiquantitative approach recently proposed by Aldini et al., which identifies those peptides undergoing a significant consumption with respect to the peptides from the native HSA.[30] In the HSA:Δ^{12}-PGJ_2 1:5 molar ratio samples, only the RHPYFYAPELLFFAK peptide underwent a consumption over ±10% (chosen as threshold level) (Supporting Information Figure S4). In particular, the peptide was reduced by almost 50%, in agreement with the relative abundance of the Δ^{12}-PGJ_2−HSA adduct, accounting for almost 50% with respect to the native HSA (calculated by baseline subtraction). On the basis of the sequence of the quenched RHPYFYAPELLFFAK peptide, the MW and the corresponding single and multicharged state ions for the Δ^{12}-PGJ_2 Michael adduct were then predicted. These predicted ion values were used as filter ions to reconstitute the SIC traces for both the native (Supporting Information Figure S5, panel A) and the Δ^{12}-PGJ_2-treated HSA (Supporting Information Figure S5, panel B). This latter molecule only contains a well detectable peak (RT = 63 min), whose MS spectrum, showing multicharged peaks at *m/z* 559.81 ($z = 4$) and *m/z* 746.08 ($z = 3$) (Supporting Information Figure S5, panel C), confirms the MW of the adducted peptide (MW = 2234.49). An MS/MS analysis was used for further confirmation and to identify the site of adduction. The MS^2 spectrum of the $[M + 2H]^{2+}$ parent ion at *m/z* 950.50 relative to the unmodified peptide (native HSA sample) is characterized by several b and y fragment ions (Figure 7A). The MS^2 spectrum of the $[M + 3H]^{3+}$ parent ion at *m/z* 746.08 relative to the Δ^{12}-PGJ_2 adduct (Figure 7B) shows the unmodified y-ion series (up to y13), and the b-ion series from the b2* ion, shifted by 336.5 Da, thus unequivocally identifying His146 as the adduction site.

Discussion

Electrophilic ligands, in addition to being noncovalently bound by the protein, have the potential to undergo nucleophilic substitution or addition reactions with the protein. Specific amino acid residues are frequently targeted by electrophilic reactants. The reasons for this site selectivity are not well understood, but most small organic molecules appear to be noncovalently bound in a specific region that contains targeted residues. If noncovalent binding, which would constrain the rotational and translational freedom of the electrophile, precedes the nucleophilic substitution reaction, it is understandable that only specific residues would be attacked. It is proposed that docking of an electrophile in a receptor region of a protein is generally the first step on the path to covalent adduct formation, and, as a result, only appropriately situated nucleophiles within the receptor are available for reaction.[31] Members of the J_2 series

(31) Skipper, P. L. *Chem. Res. Toxicol.* **1996**, *9*, 918–923.

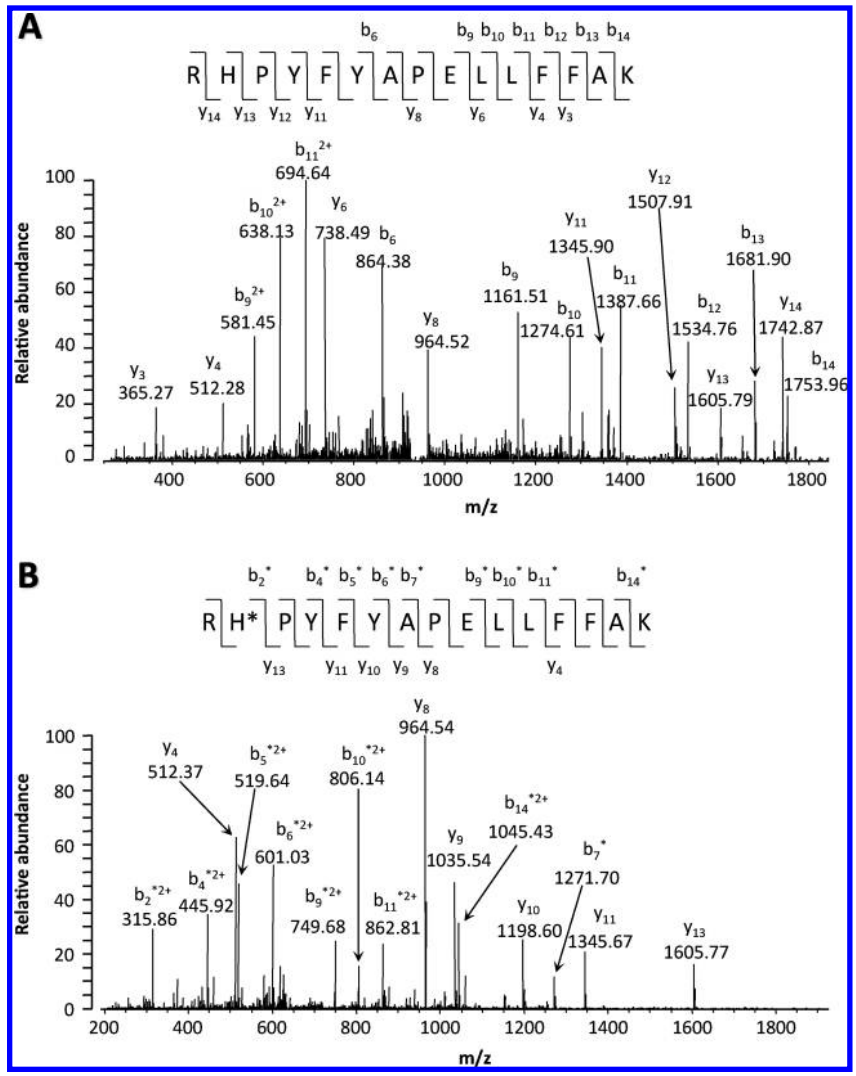

Figure 7. Identification of the Δ^{12}-PGJ$_2$-binding site using nano-LC-MS/MS. (A) LC-ESI-MS/MS spectra of native and Δ^{12}-PGJ$_2$-adducted RHPYFYAPELLFFAK peptide. LC-ESI-MS/MS spectra of native (parent ion *m/z* 950.50, upper panel) and Δ^{12}-PGJ$_2$-adducted (parent ion *m/z* 746.08, lower panel) RHPYFYAPELLFFAK peptide. His146 was identified as the adduction site. The modified fragment ions are labeled with an asterisk and according to the nomenclature of the peptide fragmentation.[60] (B) Main interactions stabilizing the complex between HSA and Δ^{12}-PGJ$_2$, which precede the covalent adduction. The dashed line underlines the closeness between the imidazole and cyclopentenone ring and confirms that such a configuration is conducive for the Michael's addition.

of the PGs, unlike other classes of eicosanoids, characterized by the presence of an electrophilic α,β-unsaturated carbonyl group in the cyclopentenone ring, have their own unique spectrum of biological effects. The reactive center of the cyPGs has been proposed to account for some of their receptor-independent biological actions.[32,33] They can covalently react via the Michael addition reaction with nucleophiles, such as the free sulfhydryls of glutathione and cysteine residues in cellular proteins that play an important role in the control of the redox cell signaling pathways.[11,32,33]

In the present study, based on the molecular interaction analysis suggesting the presence of a specific Δ^{12}-PGJ$_2$-binding site in HSA (Figure 3), we analyzed the crystal structure of the HSA$-\Delta^{12}$-PGJ$_2$ complex and identified the Δ^{12}-PGJ$_2$-binding site in HSA, which lies in a D-shaped cavity in the center of the four-helix bundle of subdomain IB (Figure 4). It was observed that two Δ^{12}-PGJ$_2$ molecules were bound within the binding pocket. No Δ^{12}-PGJ$_2$ molecule was detected at other fatty acid binding sites or coexisted with the fatty acid molecule (myristate), indicating that Δ^{12}-PGJ$_2$ could replace the fatty acid only in subdomain IB. Of interest, the electron density for the Δ^{12}-PGJ$_2$ was stronger in the HSA$-$myristate-Δ^{12}-PGJ$_2$ complex than in the HSA$-\Delta^{12}$-PGJ$_2$ complex, indicating that Δ^{12}-PGJ$_2$ might be more stably associated with the pockets in the presence of a fatty acid. It is apparent from these findings that subdomain IB is the preferred binding site for the PGD$_2$ metabolite. This site is not observed in the defatted HSA structure[34] and may occur only in the presence of significant amounts of fatty acids. Selective binding of Δ^{12}-PGJ$_2$ to subdomain IB raises the question as to why no Δ^{12}-PGJ$_2$ molecule is bound to other fatty acid-binding sites. It may be simply because, in comparison to the other major fatty acid binding pockets on the protein, subdomain IB is relatively open and accessible to solvent. Indeed, Tyr138 stacks with Tyr161 and occludes the binding pocket in the absence of fatty acid, whereas, upon fatty acid binding at this site, the tyrosine side-chains rotate through about

(32) Rossi, A.; Kapahi, P.; Natoli, G.; Takahashi, T.; Chen, Y.; Karin, M.; Santoro, M. G. *Nature* **2000**, *403*, 103–108.
(33) Bui, T.; Straus, D. S. *Biochim. Biophys. Acta* **1998**, *1397*, 31–42.
(34) He, X. M.; Carter, D. C. *Nature* **1992**, *358*, 209–215.

90° so that their phenyl rings hold the lipid in a hydrophobic clamp.[35] It has been shown that all of the fatty acids bind at this site in the same orientation with the carboxyl group hydrogen-bonded to Arg117 and to a water molecule that is also coordinated by the side-chain hydroxyl group of Tyr161 and the carbonyl oxygen atom of Leu182. The preferential binding of Δ^{12}-PGJ$_2$ to subdomain IB may be associated with the fact that the site represents a catalytic domain where PGJ$_2$ is converted to Δ^{12}-PGJ$_2$.

Crystallographic and mass spectrometric analyses of the HSA−Δ^{12}-PGJ$_2$ complex also showed that Δ^{12}-PGJ$_2$ could form a covalent adduct at His146. The docking analyses confirmed that the interdomain cleft between subdomains IB and IIA can accommodate Δ^{12}-PGJ$_2$ in a pose conducive to the Michael adduct (Figure 4B and C). The best docking configuration of Δ^{12}-PGJ$_2$ around His146 suggests that the distance between the cyclopentenone ring and the imidazole nitrogen is reasonably productive for the Michael adduction (4.7 Å). The identification of histidine as the covalent binding site of Δ^{12}-PGJ$_2$ was unexpected because the cyPGs have been considered to be totally inert to amino acids, except cysteine.[36] The Δ^{12}-PGJ$_2$-histidine Michael adduct may be stabilized toward retro-Michael reaction, on account of the poorer leaving group ability of imidazole over other functional groups, such as sulfhydryl and amine, at neutral conditions. His146 is located at the entrance of fatty acid binding site 1 in the strong nucleophilic region (Figure 4) that has been previously reported to be the adduction site of a lipid peroxidation-derived aldehyde,[30] polycyclic aromatic hydrocarbon epoxides,[37] and of the butadiene metabolite, epoxybutanediol.[38] As illustrated in Supporting Information Figure S6, His146 faces a well-known pocket in subdomain IB, which is characterized by a small number of nucleophile residues (Lys137, His146, and Lys159) with an exceptional reactivity. Even if this subdomain has not been regarded as a true drug-binding site, it is accepted that reactive aromatic electrophiles have a marked specificity for this region where they can form covalent adducts with the mentioned nucleophilic residues. Such specificity can be explained by considering that this region is particularly rich in aromatic and positively charged residues, which can favor the noncovalent binding preceding covalent bond formation. Moreover, the richness of positively charged residues can also justify the remarkably low pK_3 values of the mentioned basic residues, which favor their neutral form rendering them reactive nucleophiles to yield covalent adducts. Thus, it is likely that the presence of a high affinity-binding site of Δ^{12}-PGJ$_2$ in a specific region might be associated with the formation of an unusual covalent bond with the histidine residue.

One of the most important features of the molecular structure of serum albumin is the presence of a highly reactive free sulfhydryl group at Cys34. This residue is a major ligand-binding site for thiol-containing compounds, such as cysteine and glutathione, and for various metal ions in a reversible manner.[39,40] Circulating serum albumin contains this Cys34 in the reduced and oxidized states known as mercaptalbumin and nonmercaptalbumin, respectively. The redox conversion of serum albumin has been considered to largely participate in the maintenance of a constant redox potential in the extracellular fluids, and the value for the mercaptalbumin fraction on serum albumin might reflect the redox buffer capacity in the body. In addition, the oxidized forms of albumin have been found to be increased under several pathological conditions.[40−43] However, no modification of Cys34 was observed in the crystal structure of the HSA−Δ^{12}-PGJ$_2$ and HSA−Δ^{12}-PGJ$_2$-myristate complexes (Supporting Information Figure S3). The docking searches around Cys34 have indeed shown that the cavity lined by Cys34, whose remarkable reactivity toward α,β-unsaturated aldehydes was investigated in a previous study,[44] is too narrow to encompass the Δ^{12}-PGJ$_2$ molecule, and therefore the reactive cyclopentenone moiety of Δ^{12}-PGJ$_2$ is always situated too far from Cys34 to yield the corresponding Michael adducts (Aldini, G., unpublished observation). Thus, due to the narrowness of the cavity, Δ^{12}-PGJ$_2$ can at most insert the aliphatic chains into the cavity, but the cyclopentenone ring remains in an external position, which cannot yield covalent adducts with Cys34.

Serum albumin is synthesized in the liver, exported as a nonglycosylated protein, and is present in the blood at around 40 mg/mL (0.6 mM). It is the major transport protein for unesterified fatty acids, but is also capable of binding an extraordinarily diverse range of metabolites, drugs, and organic compounds.[16,39,45] It has also been shown that albumin can induce a variety of cellular processes that represent a cellular response program under apoptotic and inflammatory stresses. Zoellner et al. have shown that serum albumins inhibit apoptosis of endothelial cells.[46] In addition, albumin has been shown to activate the AKT pathway and promote resistance of B-chronic lymphocytic leukemia cells to DNA damage-induced apoptosis in vitro.[47] Erkan et al. have reported that albumin overload induces apoptosis in cultured proximal tubular cells, mediated at least in part by the Fas-FADD-caspase 8 pathway.[48] Albumin is taken up by the proximal tubule cells via receptor-mediated endocytosis and can induce the expression of several inflammatory molecules. This complex mixture of inflammatory substances induced by albumin may contribute to a number of cellular events associated with immune and inflammatory processes. However, the potential role of albumin, or its multiple ligands, on the regulation of cellular functions has not been fully explored.

cyPGs, such as Δ^{12}-PGJ$_2$ and 15d-PGJ$_2$, emerged as a likely regulator of acute and chronic inflammation. The anti-inflam-

(35) Curry, S.; Brick, P.; Franks, N. *Biochim. Biophys. Acta* **1999**, *1441*, 131–140.
(36) Suzuki, M.; Mori, M.; Niwa, T.; Hirata, R.; Furuta, K.; Ishikawa, T.; Noyori, R. *J. Am. Chem. Soc.* **1997**, *119*, 2376–2385.
(37) Brunmark, P.; Harriman, S.; Skipper, P. L.; Wishnok, J. S.; Amin, S.; Tannenbaum, S. R. *Chem. Res. Toxicol.* **1997**, *10*, 880–886.
(38) Lindh, C. H.; Kristiansson, M. H.; Berg-Andersson, U. A.; Cohen, A. S. *Rapid Commun. Mass Spectrom.* **2005**, *19*, 2488–2496.
(39) Carter, D. C.; Ho, J. X. *Adv. Protein. Chem.* **1994**, *45*, 152–203.
(40) Kawai, K.; Yoh, M.; Hayashi, T.; Imai, H.; Negawa, T.; Tomida, M.; Sogami, M.; Era, S. *Tokai J. Exp. Clin. Med.* **2001**, *26*, 93–99.
(41) Tomida, M.; Ishimaru, J.; Hayashi, T.; Nakamura, K.; Murayama, K.; Era, S. *Jpn. J. Physiol.* **2003**, *53*, 351–355.
(42) Mera, K.; Anraku, M.; Kitamura, K.; Nakajou, K.; Maruyama, T.; Otagiri, M. *Biochem. Biophys. Res. Commun.* **2005**, *334*, 1322–1328.
(43) Musante, L.; Bruschi, M.; Candiano, G.; Petretto, A.; Dimasi, N.; Del Boccio, P.; Urbani, A.; Rialdi, G.; Ghiggeri, G. M. *Biochem. Biophys. Res. Commun.* **2006**, *349*, 668–673.
(44) Aldini, G.; Vistoli, G.; Regazzoni, L.; Gamberoni, L.; Facino, R. M.; Yamaguchi, S.; Uchida, K.; Carini, M. *Chem. Res. Toxicol.* **2008**, *21*, 824–835.
(45) Kragh-Hansen, U. *Danish Med. Bull.* **1990**, *37*, 57–84.
(46) Zoellner, H.; Höfler, M.; Beckmann, R.; Hufnagl, P.; Vanyek, E.; Bielek, E.; Wojta, J.; Fabry, A.; Lockie, S.; Binder, B. R. *J. Cell Sci.* **1996**, *109*, 2571–2580.
(47) Jones, D. T.; Ganeshaguru, K.; Anderson, R. J.; Jackson, T. R.; Bruckdorfer, K. R.; Low, S. Y.; Palmqvist, L.; Prentice, H. G.; Hoffbrand, A. V.; Mehta, A. B.; Wickremasinghe, R. G. *Blood* **2003**, *101*, 3174–3180.
(48) Erkan, E.; De Leon, M.; Devarajan, P. *Am. J. Physiol. Renal. Physiol.* **2001**, *280*, F1107–F1114.

matory effect was first deduced from an animal model of carrageenin-induced inflammation in which a two-phase PG release has been described after the expression of COX-2; the PGE_2 synthesis predominates during the early inflammatory step, whereas 15d-PGJ_2 substitutes for the PGE_2 formation at the end of the process, coincident with the accumulation of macrophages.[12] Cuzzocrea et al. also demonstrated the effects of 15d-PGJ_2 in rodent models of chronic collagen-induced arthritis inflammation.[13] In a later study, Itoh et al. showed that the accumulation of 15d-PGJ_2 activates Nrf2 and regulates the inflammation process through the induction of a target gene expression.[14] On the basis of these findings, the physiopathological relevance of the enhanced synthesis of cyPGs in activated macrophages has been speculated to represent a mechanism, in which they function as a feedback regulator of the inflammatory responses. Of interest, our recent study has revealed that the HSA−Δ^{12}-PGJ_2 complexes markedly induce the gene expression of pro-inflammatory molecules, such as COX-2.[49] These observations suggest that the cyPGs, at least Δ^{12}-PGJ_2, might have pro-inflammatory roles and challenges the concept that they are exclusively involved in the anti-inflammatory responses. Future studies are required to determine whether and how the enhanced production of the cyPGs, Δ^{12}-PGJ_2 in particular, could be functionally associated with inflammatory processes and the net effect in vivo of the interplay between the anti- and pro-inflammatory products of COX in human diseases.

Experimental Section

Materials. HSA (fatty acid and globulin free, purity 99%) was obtained from Sigma-Aldrich. Δ^{12}-PGJ_2 and free fatty acids were purchased from the Cayman Chemical Co. (Ann Arbor, MI). The protein concentration was measured using the BCA protein assay reagent obtained from Pierce. The sequence grade modified trypsin was obtained from Promega (Milan, Italy). The LC-MS grade solvents (Chromasolv) were purchased from Sigma-Aldrich (Milan, Italy).

In Vitro Modification of Isolated HSA by Δ^{12}-PGJ_2. Blood collected by venopuncture from two healthy male volunteers was allowed to clot at room temperature for no longer than 30 min and then centrifuged for 10 min at 1500*g*. The serum aliquots were then stored in liquid nitrogen until used. Serum albumin was isolated using the Affi-gel blue-gel (Biorad, Milan, Italy) and eluted with 1.4 M NaCl in 20 mM phosphate buffer saline (PBS, pH 7.2). The HSA concentration was measured by absorbance at 279 nm (E1% 1 cm = 5.31). The samples were then desalted on YM30 Microcon centrifugal filter devices (Millipore, Milan, Italy) by rinsing with distilled water, and diluted with 20 mM PBS (pH 7.4) to a final concentration of 40 μM. Δ^{12}-PGJ_2 dissolved in methanol was then added to obtain the final HSA:Δ^{12}-PGJ_2 molar ratios of 1:1 and 1:5. After a 180 min incubation at 37 °C, the samples were analyzed by direct infusion mass spectrometry as detailed below. Additional samples were then incubated at room temperature for an additional 60 min with $NaBH_4$ (final concentration 5 mM), and then desalted by Microcon filter devices as already described, lyophylized, and stored in liquid nitrogen until enzyme digestion.

Surface Plasmon Resonance. The binding of Δ^{12}-PGJ_2 to HSA was measured by a Biacore T100 system at 25 °C and a flow rate of 100 μL/min. HSA (3800 response units) was immobilized on a CM5 surface via covalent linkage to the N terminus of HSA. A CM5 chip was activated using 1:4 *N*-hydroxysuccinimide (NHS)/1-ethyl-3-(3-dimethylaminopropyl)carbodiimide (EDC) at the flow rate of 10 μL/min for 7 min. HSA (20 μg/mL) in 10 mM acetate buffer (pH 5.5) was passed over separate flow cells at 10 μL/min for 3 min, and this was followed by a blocking step using ethanolamine (1 M, pH 8.5) at 10 μL/min for 7 min. Binding studies were performed by passing Δ^{12}-PGJ_2 over the immobilized HSA at the flow rate of 10 μL/min. The association and dissociation times were 60 and 60 s, respectively. The running buffer contained 150 mM NaCl, 10 mM HEPES, 3 mM EDTA, 0.05% (v/v) surfactant P-20, pH 7.4, and 5% DMSO. The complex formation between Δ^{12}-PGJ_2 and the immobilized protein was measured with 3.0−500 μM of ligand in the running buffer. A sample volume of 20−40 μL was injected into the flow cell. Dissociation of the bound ligand was initiated by injecting running buffer without any ligand.

Protein Purification, Complex Formation, and Crystallization. The protocol was based on a previously developed method for formation of the HSA−myristate complex.[17] The HSA fraction V fatty acid free (Sigma-Aldrich) was further purified by anion-exchange chromatography on UNO Q-6 (Bio-Rad Laboratories) pre-equilibrated with buffer A (20 mM phosphate buffer, pH 7.0). The protein was eluted with a linear gradient of NaCl (0−0.5 M). The fractions containing HSA were pooled, then applied onto a HiTrap desalting column (GE Healthcare) pre-equilibrated in buffer A to remove the NaCl. The purified protein was concentrated to 100 mg/mL using the Vivaspin 6 concentrator (10-kDa molecular-weight cutoff, Sartorius). Myristate (Wako, Osaka, Japan) dissolved in buffer A was heated to 50 °C to facilitate the dispersal of myristate, and then mixed with solution containing HSA to achieve the myristate molar ratio of 4. To gain the tertiary complex of HSA, myristate, and Δ^{12}-PGJ_2, the Δ^{12}-PGJ_2 solution (Cayman Chemical) was concentrated under a gentle stream of nitrogen, and then a 5-fold molar excess of Δ^{12}-PGJ_2 was directly dissolved in the HSA−myristate solution. Crystals were obtained by the vapor diffusion hanging drop technique against a reservoir solution containing 50 mM phosphate buffer, pH 6.5−7.0, 28−32% (w/v) PEG 3350. Colorless crystals with the dimensions of 0.5 × 0.5 × 1.0 mm grew within 2 weeks. The crystals were harvested by the gradual addition of 2 μL of cryoprotectant solution containing Δ^{12}-PGJ_2 and slightly higher PEG 3350 concentrations than were used for crystallization to the hanging drop. The diffraction data were collected at 98 K using the beamline BL5A of the Photon Factory (Tsukuba, Japan).

Data Collection and Structure Determination. Diffraction images of the data set were indexed, integrated, and scaled with the HKL2000 program suite.[50] The crystals are in the space group *P*1, with unit cell dimensions $a = 38.1$, $b = 92.1$, $c = 94.7$, $\alpha = 74.8°$, $\beta = 89.5°$, $\gamma = 80.2°$, and contain two molecules (chain A/B) in the asymmetric unit. The initial phases were obtained by molecular replacement with the program Phaser in the CCP4 program suite.[51] The search model stripped of its myristate was taken from the PDB code 1BJ5. Model building in the electron density map and crystallographic refinement were performed using the programs in the CCP4 program suite and Coot.[52] After cycles of restrained refinement and manual adjustments, the resulting electron density maps were used to guide positioning of the ligands and bound water molecules and further refined in Refmac using 3 TLS groups.[53] The omit map was also calculated using the program Sfcheck to reduce the model bias in the electron density.[54] The final model, refined to 2.2□, contains two proteins, three Δ^{12}-PGJ_2, 12 myristic acids, and the solvent molecules. The surface electrostatic potentials of the PTP1Bs were calculated by the Poisson−

(49) Morishita, N.; Shibata, T.; Ito, S.; Carini, M.; Aldini, G.; Uchida, K., to be submitted.

(50) Otwinowski, Z.; Minor, W. *Methods Enzymol.* **1997**, *276*, 307–326.
(51) Collaborative Computational Project, Number 4, The CCP4 suite: programs for protein crystallography. *Acta Crystallogr., Sect. D* **1994**, *50*, 760−763.
(52) Emsley, P.; Cowtan, K. *Acta Crystallogr., Sect. D* **2004**, *60*, 2126–2132.
(53) Vagin, A. A.; Steiner, R. A.; Lebedev, A. A.; Potterton, L.; McNicholas, S.; Long, F.; Murshudov, G. N. *Acta Crystallogr., Sect. D* **2004**, *60*, 2184–2195.
(54) Vaguine, A. A.; Richelle, J.; Wodak, S. J. *Acta Crystallogr., Sect. D* **1999**, *55*, 191–205.

Boltzmann equation as implemented in the eF-surf server,[55] and all figures were prepared using MolFeat (FiatLux Co.) and Coot. The coordinates and structure factors have been deposited in the Protein Data Bank (ID code is 3A73). To evaluate the ligand−protein interactions within the asymmetric unit, we utilized the Protein Interfaces, Surfaces and Assemblies (PISA) service.[56] The data collection and refinement statistics are summarized in Supporting Information Table S1.

Mass Spectrometry. Direct Infusion Electrospray Mass Spectral Analysis (ESI-MS): Linear Ion Trap Mass Spectrometer. To detect changes in the protein mass and to determine the stoichiometry of the reaction, undigested native and Δ^{12}-PGJ$_2$-treated HSA were analyzed by direct infusion using an LXQ Linear Ion Trap mass spectrometer (Thermo Scientific, Milan, Italy) equipped with an Electrospray Finnigan Ion Max source. Lyophilized protein (500 μg) was dissolved in 200 μL of water, mixed with 200 μL of $CH_3CN-H_2O-HCOOH$ (60:40:0.4, v/v/v), and infused into the mass spectrometer at the flow rate of 3 μL/min. Each sample was analyzed using two different mass ranges, *m/z* 600−2000 and *m/z* 1410−1500, under the following instrumental conditions: positive ion mode, 350 °C capillary temperature; 3.5 kV spray voltage applied to the needle, 46 V capillary voltage, nebulizer gas (nitrogen) flow rate set at 20 (au), and 5 min acquisition.

Nano-LC-MS/MS Analysis. Peptide maps were generated by nano-LC-ESI-MS/MS analysis in data-dependent scan mode and dynamic exclusion in positive-ion mode. For the sample preparation, the lyophilized target protein was dissolved in 100 μL of 50 mM Tris-HCl (pH 7.8) and digested according to the manufacturer's procedure. Two microliter aliquots of the digested samples were diluted 1:100 with 0.1% formic acid and injected into a quaternary pump HPLC system (Surveyor LC system, ThermoQuest, Milan, Italy). All of the digested peptide mixtures were separated by online reversed-phase (RP) nanoscale capillary liquid chromatography (nanoLC) and analyzed by electrospray tandem mass spectrometry (ESI-MS/MS). Chromatography was performed using a Surveyor LC system (ThermoFinnigan Italia, Milan, Italy) on a 180 μm × 10 cm column packed with 5 μm, Biobasic-18 stationary phase (Thermo, Superchrom, Milan, Italy). The pump flow rate was split 1:75 for a column flow rate of 2 μL/min. The column effluent was directly electrosprayed using the silica emitter source without further splitting. Mobile phases A and B were 0.1% formic acid in water and in acetonitrile, respectively. The separation of the peptides obtained by enzymatic digestion was achieved with a gradient of 0−60% B over 60 min. Before the next analysis, both the precolumn and the column were first washed with 90% solvent B for 10 min and then equilibrated with 100% solvent A for 20 min. For the identification of the peptides, an LTQ XL-Orbitrap mass spectrometer was used (Thermo Scientific, Milan, Italy), and the electrospray interface (dynamic nanospray probe, Thermo Scientific, Milan, Italy) was set as follows: 1.5 kV spray voltage; 180 °C capillary temperature, 30 V capillary voltage; 110 V tube lens offset, and no sheath or auxiliary gas flow. During the analysis, the mass spectrometer continuously performed scan cycles in which a high-resolution (resolution $r = 30\,000$ at *m/z* 400) full scan (300−2000 *m/z*) in the profile mode was first made by the Orbitrap, after which the MS2 spectra were recorded in the centroid mode for the three most intense ions (isolation width, 3 *m/z*; normalized collision energy, 30 CID arbitrary units). Protonated phthlates [dibutylphthlate (plasticizer), *m/z* 279.159086; bis(2-ethylhexyl)phthalate, *m/z* 391.284286] and polydimethylcyclosiloxane ions [$(Si(CH_3)_2O)_6 + H]^+$; *m/z* 445.120025] were used for the real time internal mass calibration. Dynamic exclusion was enabled (repeat count, 3; repeat duration, 10 s; exclusion list size, 25; exclusion duration, 120 s; relative exclusion mass width, 5 ppm). Charge state screening and monoisotopic precursor selection were enabled, and singly and unassigned charged ions were not fragmented.

Peptide Adduct Identification. Peptide ion responses were determined by measuring the peak areas in the selected ion chromatograms (SICs) reconstituted using the most abundant multicharged ion as the filter ion as previously reported.[57] The peptide responses were normalized with respect to the LVAASQAALGL peptide, chosen as the reference peptide because it does not contain nucleophilic residues that can be adducted by Δ^{12}-PGJ$_2$. The loss of specific peptides in the Δ^{12}-PGJ$_2$-treated HSA with respect to the native HSA was determined by calculating the relative peptide consumption using the following equation: peptide consumption (%) $= 100 - [(A_{12\text{-dPGJ2}})/(A_{\text{NATIVE}}) \times 100]$, where $A_{12\text{-dPGJ2}}$ and A_{NATIVE} are the normalized peptide ion responses of the target peptide from HSA incubated in the presence and in the absence of Δ^{12}-PGJ$_2$, respectively.

Bioinformatics. The direct infusion ESI-MS spectra were deconvoluted using the software packages Bioworks 3.1 (ThermoQuest, Milan, Italy) and MagTran 1.02.[58] The peptide sequences were identified using the software turboSEQUEST (Bioworks 3.1, ThermoQuest, Milan, Italy) and using a database containing only the protein of interest and assuming trypsin digestion. The in silico tryptic digest of HSA was also used as an aid for peptide identification. The protein sequence of HSA was obtained from the SWISS-PROT database (primary accession number P02768). PEPTIDEMASS was used to calculate the theoretical digested masses on the basis of the tryptic digest and setting all the Cys as carbamidomethyl-cysteine. The predicted y and b series ions were determined using the Peptide Sequence Fragmentation Modeling, Molecular Weight Calculator software program (ver. 6.37), http://come.to/alchemistmatt. The Xcalibur software provided the instrument control and data analysis of the Thermo Electron mass spectrometers.

Acknowledgment. This work was supported by a Grant-in-Aid for Scientific Research on Innovative Areas (Research in a Proposed Research Area), MEXT, Japan (K.U.), and by MIUR (Ministero dell'Istruzione, dell' Università e della Ricerca), Italy (PRIN 2007).

Supporting Information Available: Supplementary figures for X-ray crystallography and mass spectrometry, and a supplementary table listing data collection and refinement statistics. This material is available free of charge via the Internet at http://pubs.acs.org.

JA908878N

(55) Kinoshita, K.; Nakamura, H. *Bioinformatics* **2004**, *20*, 1329–1330.
(56) Krissinel, E.; Henrick, K. *J. Mol. Biol.* **2007**, *372*, 774–797.
(57) Aldini, G.; Gamberoni, L.; Orioli, M.; Beretta, G.; Regazzoni, L.; Maffei Facino, R.; Carini, M. *J. Mass Spectrom.* **2006**, *41*, 1149–1161.
(58) Zhang, Z.; Marshall, A. G. A. *J. Am. Soc. Mass Spectrom.* **1998**, *9*, 225–23.
(59) Petitpas, I.; Grune, T.; Bhattacharya, A. A.; Curry, S. *J. Mol. Biol.* **2001**, *314*, 955–960.
(60) Biemann, K. *Biomed. Environ. Mass Spectrom.* **1988**, *16*, 99–111.